Macromolecules
ARTICLE

Macromolecules **2010**, *43*, 9411–9416 **9411**
DOI: 10.1021/ma101456y

Alternate Multilayer Films of Poly(vinyl alcohol) and Exfoliated Graphene Oxide Fabricated via a Facial Layer-by-Layer Assembly

Xin Zhao, Qinghua Zhang,* Yanping Hao, Yingzhi Li, Ying Fang, and Dajun Chen

State Key Laboratory for Modification of Chemical Fibers and Polymer Materials, College of Materials Science and Engineering, Donghua University, Shanghai 201620, P. R. China

Received June 30, 2010; Revised Manuscript Received September 18, 2010

ABSTRACT: Despite great recent progress with graphene-based materials, the development of strong and cost-efficient multifunctional graphene-filled polymer composites has not yet to be achieved. A key challenge in the fabrication of nanoplatelet-filled polymer composites is the ability to realize the nanometer-level dispersion and the planar orientation of nanosheets in polymer matrices. In this report, ultrathin multilayer $(PVA/GO)_n$ films were successfully fabricated by bottom-up layer-by-layer (LBL) assembly of poly(vinyl alcohol) (PVA) and exfoliated graphene oxide (GO), in which exfoliated GO nanosheets were used as the building blocks. Typical tapping-mode atomic force microscope (AFM) and field emission scanning electron microscope (FESEM) images demonstrate an ordered arrangement of organic and inorganic layers. A significant enhancement of mechanical properties has been achieved, that is, a 98.7% improvement of elastic modulus (E_r) and a 240.4% increase of hardness. This may be attributed to the well-defined layered architecture with high degree of planar orientation and nanolevel assemblies of GO nanosheets in the polymer matrices.

1. Introduction

Graphene-based materials have attracted a tremendous amount of attention in many areas on science and engineering due to the excellent properties of graphene sheets.[1−8] As determined by theoretical and experimental results, individual graphene nanosheets exhibit extremely high values of Young's modulus (~1000 GPa), fracture strength (~125 GPa),[1] elastic modulus (~0.25 TPa),[2] thermal conductivity (~5000 W m^{-1} K^{-1}),[3] mobility of charge carriers (~200 000 cm^2 V^{-1} s^{-1}),[4] specific surfaced area (calculated value ~2630 m^2 g^{-1}),[5] and fascinating transport phenomena such as the quantum Hall effect.[6] The structure of graphene oxide (GO) is often simplistically assumed to be a graphene sheet bonded to oxygen in the form of carboxyl, hydroxyl, and epoxy groups,[7−9] providing more possibilities for applications in materials science and nanocomposites.[10−13]

One of the key issues to successful development of nanoplatelet-filled polymer nanocomposites is the nanometer-level dispersion and the orientation of nanosheets in polymer matrices. Li et al.[14] reported that chemically converted graphene nanosheets obtained from graphite could readily form stable aqueous colloids through electrostatic stabilization. Stankovich et al.[15] treated GO with organic isocyanates, and these isocyanate-treated GO exhibit a stable dispersion in polar aprotic solvents. So molecular-level dispersion of individual, chemically modified graphene sheets within polymer hosts could be fabricated.[10] This group[16] also reported a stable aqueous dispersion of graphitic nanoplatelets by coating reduced graphene oxide nanoplatelets with an amphiphilic polymer. Liang et al.[17] fabricated graphene-based poly(vinyl alcohol) nanocomposites with molecule-level dispersion, and there were a 76% increase in tensile strength and a 62% improvement of Young's modulus.

*Corresponding author: e-mail qhzhang@dhu.edu.cn; Fax 0086 21 67792854.

In the methods of fabricating organic−inorganic nanocomposites, layer-by-layer (LBL) has been widely accepted because it is a simple, powerful, and environmental approach for assembling functional building blocks into ultrathin films with controlled type, size, morphology, internal organization, and molecular structure on planar solid substrates.[18,19] LBL assembly has successfully been extended to several different kinds of driving forces, such as electrostatic forces,[20] hydrogen bonding,[21−24] covalent bonding[25,26] and other weak intermolecular interactions. Recent increasing interests focus on the construction of nanoscale LBL assembled materials driven by hydrogen bond formation, opening a new opportunity for the LBL technique.[27−33]

In this report, we fabricated ultrathin poly(vinyl alcohol) PVA/GO composite films by LBL self-assembly, in which exfoliated GO nanosheets were used as building blocks. The existence of oxygen functional groups located on both edges and basal plane of GO and the hydroxyl groups in PVA chains makes it possible to fabricate layer-by-layer ultrathin films by hydrogen-bonding interaction. Unlike our previous report,[34] in which random orientation grephene/PVA nanocomposite was prepared by a simply solution blends, alternative deposition of PVA and GO nanolayers results in a uniform growth of films containing high planar orientation and good dispersion of inorganic nanofillers. To the best of our knowledge, this is the first report of multilayer ultrathin films of graphene-like materials and polymer through the LBL technique.

2. Experimental Section

2.1. Materials. Graphite with an average particle size of 30 μm and a purity of >99% were supplied from Shanghai Yifan's graphite Co., Ltd. Poly(vinyl alcohol) (PVA) with $M_w \sim 100\,000$ was obtained from Anhui Wanwei Updated High-Tech Material Industry Co., Ltd. Concentrated sulfuric acid (H_2SO_4) and hydrochloric acid (HCl) were purchased from Pinghu Chemicals, China. Potassium permanganate ($KMnO_4$) was purchased

Published on Web 10/28/2010

from Reagent No. 1 Factory of Shanghai Chemical Reagent Co., Ltd. Sodium nitrate ($NaNO_3$) was purchased from Shanghai Kechuang Chemicals Co., Ltd. Hydrogen peroxide (H_2O_2) was purchased from Shanghai Jinlu Chemical Co., Ltd. Barium chloride ($BaCl_2$) and 25 wt % glutaraldehyde solution were purchased from Sinopharm Chemical Reagent Co., Ltd. The materials were directly used without further purification.

2.2. Fabrication of GO. Graphite oxide, a pseudo-two-dimensional solid in bulk form, was prepared from natural graphite powder by oxidation with $KMnO_4$ in concentrated H_2SO_4 according to Hummers' method. Concentrated H_2SO_4 (46 mL) was poured into the 250 mL three-neck flask and stirred in an ice bath until the temperature dropped to 0−3 °C. Natural graphite (2 g) and $NaNO_3$ (1 g) were added and stirred uniformly. $KMnO_4$ (6 g) was added gradually with stirring and cooling in order to keep the temperature below 20 °C. The solution was heated to 35 ± 3 °C and maintained for 30 min. Then, distilled water (92 mL) was slowly added, and the temperature was controlled lower than 100 °C. After 15 min, this reaction was terminated by adding distilled water (150 mL) and 30% H_2O_2 solution (5 mL). The mixture was filtered and washed successively with 5% HCl aqueous solution completely until sulfate could not be detected with $BaCl_2$. The sample of graphite oxide was thus obtained after drying.

2.3. Fabrication of Films. 1 wt % PVA solution used for LBL assembly was prepared by dissolving 2 g of PVA powder in 200 mL of 80 °C deionized water under vigorous stirring for ~3 h. Yellow-brown dispersion of exfoliated graphene oxide was prepared by dissolving 20 mg of graphite oxide in 200 mL of deionized water by sonication with a cylindrical tip for 30 min. After sonication, the insoluble fraction was allowed to sediment and supernatant was collected. Prior to deposition of the PVA−GO films, the glass slides and silicon wafers were cleaned by immersing into "piranha" solution (3:1 H_2SO_4:H_2O_2) for 1 h. This process also could initiate some silicon-bound hydroxyl groups on the surface of quartz substrates. The cleaned substrates were thoroughly rinsed with deionized water and dried under air flow. The overall process of LBL deposition of heterogeneous ultrathin film of $(PVA/GO)_n$ consists of a cyclic repetition of the following steps: (1) dipping the treated glass slide into 1 wt % PVA for 5 min; (2) rinsing with deionized water thoroughly for 2 min and gently dried with air flow; (3) immersing into 0.1 mg/mL GO dispersion for 5 min; (4) rinsing with deionized water for 2 min and again gently dried with air flow. This procedure gave a single deposition cycle, and the cycle could then be repeated as necessary to obtain the desired number of bilayers $(PVA/GO)_n$. In order to prevent cross-contamination risk and strengthen the combination between organic particles and polymer matrices, film with every 10 bilayers were immersed into 5 vol % solution of glutaraldehyde for 30 min to allow for cross-linking. A parallel pure PVA film was prepared by the method as mentioned above.

2.4. Characterization. The UV−vis absorption spectra were measured on a Lambda 35 (Perkin-Elmer) spectrophotometer. Raman spectra were recorded using a LabRam-1B Raman spectroscope with He−Ne laser excitation at 632.8 nm, scanning for 50 s. X-ray diffraction (XRD) measurements were carried out using a Rigaku D-max-2550 diffractometer with Cu Kα radiation (λ = 0.1514 nm). A typical tapping-mode atomic force microscope (AFM) measurement was taken using Multimode SPM from Digital Instruments with a Nanoscope IV controller made by Veeco Instruments Inc. The fracture surface morphology of the composite was observed on a Hitachi S-4800 at an accelerating voltage of 10 kV. The sample was deposited on glass slides, fractured in liquid nitrogen, and carbon-sputtered prior to observation. X-ray photoelectron spectroscopy (XPS) experiments were carried out on a RBD upgraded PHI-5000C ESCA system (Perkin-Elmer) with Mg Kα radiation ($h\nu$ = 1253.6 eV) or Al Kα radiation ($h\nu$ = 1486.6 eV). The data analysis was carried out by means of RBD AugerScan 3.21 software provided by RBD Enterprises. The surface topography image was observed on Wyko NT9100 optical profiler made by Veeco Instruments Inc. The measurement of the mechanical properties was carried out by the TriboIndenter in-situ nanomechanical test system from Hysitron, Inc.

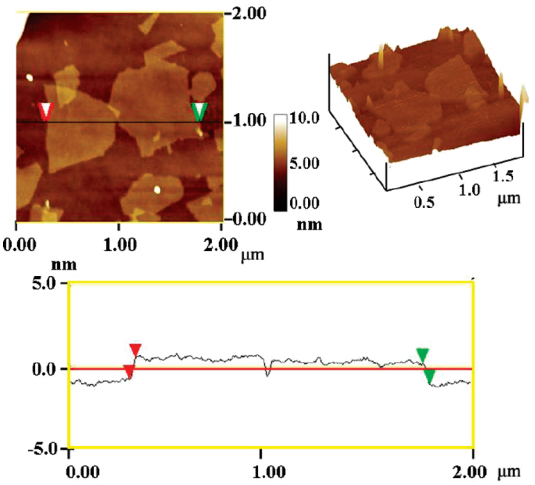

Figure 1. A typical AFM tapping-mode image of graphene oxide nanosheets deposited onto a mica substrate from an aqueous dispersion with superimposed cross-section measurements taken along the red line, indicating a sheet thickness of ~1.3 nm.

3. Results and Discussion

3.1. Exfoliation of Graphene Oxide. Graphite oxide, a pseudo-two-dimensional solid in bulk form, was prepared from natural graphite powder by oxidation with $KMnO_4$ in concentrated H_2SO_4 according to Hummers' method.[35] With many oxygen-containing functional groups, GO can be well dispersed in water at the level individual sheets in our work. Figure 1 exhibits a typical tapping-mode AFM image of GO nanosheets deposited onto a mica substrate from an aqueous dispersion. Analysis of a large number of AFM images shows most GO nanosheets had heights of ~1.3 nm and length in the range of ~1 μm. This fact reveals characteristics of fully exfoliated graphene oxide nanosheets.[36]

X-ray diffraction determines the changes of interlayer distance in nanosheets.[34] The diffraction peak in the XRD pattern of graphite oxide is appeared to 11.3°, corresponding to the layer-to-layer distance of ~0.78 nm. It is significantly larger than that of pristine graphite (~0.34 nm), owing to the intercalating oxide functional groups.[37] The D band at ~1340 cm^{-1} and G band at ~1581 cm^{-1} were observed in Raman spectroscopy for graphite oxide. The D band becomes prominent, and the ratio of D- to G-band intensity (I_D/I_G) increases from 0.14 for pristine graphite to 1.23 for graphite oxide, which reveals the process of oxidation of graphite. The 2D band at 2680 cm^{-1} of graphite oxide broadens and decreases in relative intensity, indicating the presence of defects in graphitic materials.[38]

X-ray photoelectron spectroscopy (XPS) and elemental analysis were employed to investigate the surface chemical states and oxidation degree of graphite oxide. As reported in Wang's paper,[39] it is necessary to characterize the oxidation degree of graphene because it concerns the suspension stability of solution. The wide scan XPS spectra of pristine graphite and graphite oxide are shown in Figure 2a,b. The elemental analysis illustrates that C/O atomic ratio (20.7) of pristine graphite is much higher than that (2.3) of graphite oxide, which demonstrates that oxidation of pristine graphite

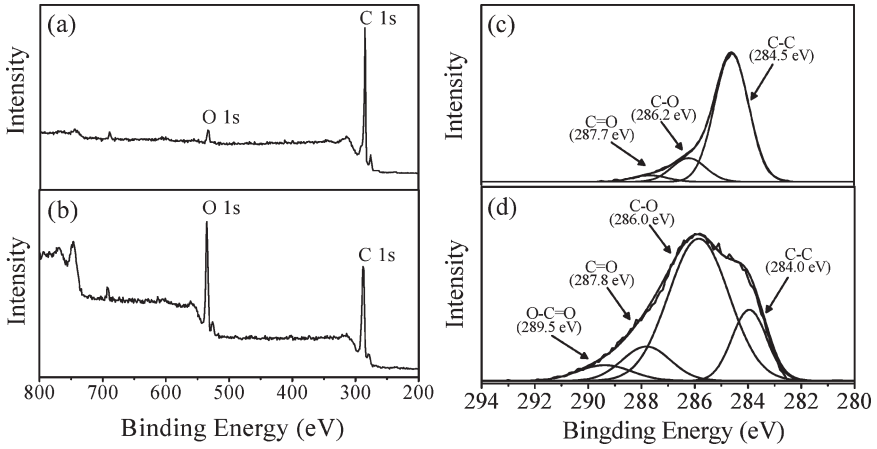

Figure 2. Wide scan XPS spectra of pristine graphite (a) and graphite oxide (b) and carbon 1s XPS spectra of pristine graphite (c) and graphite oxide (d).

is successfully conducted.[40] This result can further be confirmed by the C 1s XPS spectrum in Figure 2c,d. The C 1s XPS spectrum of graphite oxide clearly indicates a considerable degree of oxidation with four components corresponding to carbon atoms in different functional groups:[17,41,42] non-oxygenated ring C (C−C of sp^2 carbon, 284.0 eV), C in C−O bonds (286.0 eV), carbonyl C (C═O, 287.8 eV), and carboxylate carbon (O−C═O, 289.5 eV). Although the C 1s XPS spectrum of pristine graphite exhibits the same oxygen functionalities that have been assigned for graphite oxide, the peak intensities of these components are much smaller than those in the graphite oxide. It is calculated that weight percentage of non-oxygenated C in pristine graphite (85%) is much higher than that (20%) in graphite oxide, revealing the oxidation degree.

3.2. Morphology and Structure of Multilayer $(PVA/GO)_n$ Films. A traditional layer-by-layer deposition process[43] of sequentially coating a surface with PVA and GO nanosheets by immersing a glass substrate in dilute solutions of the components is employed to prepare the films. PVA, an uncharged and water-soluble polymer, is used in the traditional electrostatic LBL technique. Nevertheless, carbon-bound hydroxyl groups in each unit of PVA can associate with the silicon-bound surface hydroxyl group of the quartz substrate and the oxidation functional groups of graphene oxide, which have been proved above to form hydrogen bonds, just as indicated schematically in Figure 3. It is supposed that the hydrogen-bonding interactions between GO nanosheets and PVA can drive the reproducible layer-by-layer composite deposition to fabricate ordered inorganic/organic periodic nanostructure, which would have analogies with the brick-and-mortar arrangement.[44]

The assembling growth of PVA/GO multilayer films was monitored by UV−vis absorption spectra and measured typically after the deposition of each cycle. A deposited unit of $(PVA/GO)_n$ is defined as two layers of PVA and GO, and n is the number of deposition cycle. Figure 4 shows the UV−vis absorption spectra of $(PVA/GO)_n$ multilayer film prepared on quartz slides with the first 10 units. The strong adsorption band at 300 nm is attributed to $n \rightarrow \pi^*$ transitions of C═O bonds at the edges of GO nanosheets.[36] A progressive increase in absorbance at this wavelength is visible with the number of bilayers increasing. The linear relationship between the absorbance and the number of deposition cycles shown in Figure 4 (inset) indicates a reproducible and uniform LBL assembly process.

FESEM images of the $(PVA/GO)_{50}$ film reveal a high degree of GO nanosheets ordering into a well-defined lamella

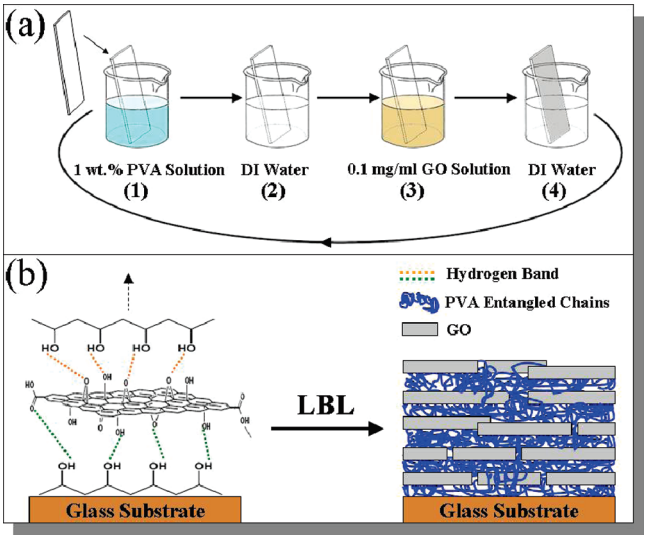

Figure 3. (a) Schematic of the composite film deposition process using glass substrate. The basic buildup sequence for the simplest film architecture $(A/B)_n$ includes four steps: (1) and (3) represent the adsorption of PVA and GO nanosheets, respectively, and (2) and (4) refer to wash steps. The cycle could be repeated as necessary to obtain the desired number of bilayers $(PVA/GO)_n$. (b) Simply schematic representation of the assembling process (left) with an interaction of GO surface and PVA macromolecular chains and the internal architecture of the PVA/GO ultrathin (right).

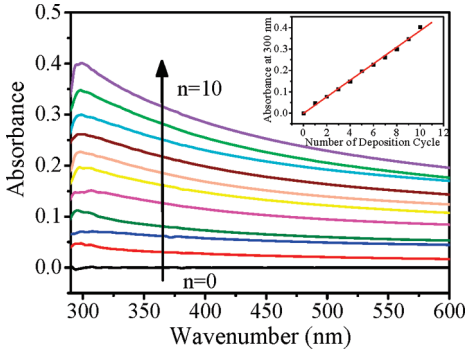

Figure 4. UV absorption spectra of $(PVA/GO)_n$ films. The number of bilayer is 1 through 10 from the bottom to the top. Inset: absorbance at 300 nm is plotted against the number of deposition cycles.

structure, which is conceptually similar to that of nacre, as shown in Figure 5. Apparently, the dense and uniform

50-bilayer film is further observed about 150 nm of the thickness.

Optical images of $(PVA/GO)_n$ ultrathin films deposited on cleaned glass substrates display that the films have a high level of flatness and homogeneity and the transparency decreases as increasing deposited cycle in Figure 6a. The highly accurate 3D surface topography for the $(PVA/GO)_{50}$ assembling film measured by optical profiling sensor technology exhibits the roughness (R_a) of film of ~0.03 μm and the thickness of ~150 nm, indicating a high degree of smoothness and an average thickness of ~3 nm for per bilayer, as shown in Figure 6b,c.

Figure 7 shows the tapping-mode AFM image of one PVA/GO unit deposited on silicon wafers, verifying dense coverage of the nanoplatelets and their strictly planar orientation. The image demonstrates that the GO nanosheets are fully exfoliated and clearly well-dispersed in the PVA matrix. It reveals that GO nanoplatelets become oriented parallel to the surface to maximize the attractive energy just like clay platelets,[44] which is different from the nanocomposites fabricated via aqueous solution in our previous report.[34] The height of GO nanosheets in the first deposited cycle, ~1.5 nm, is slightly larger than that of GO nanosheets in solution (shown in Figure 1), which may be attributed to the adsorption of polymer chains. However, as the number of bilayers increases, the contours of GO nanoplatelets become blurred and the height has no measurable value because of the entanglement of polymer chains, as shown in Figure 7b of five deposited cycle.

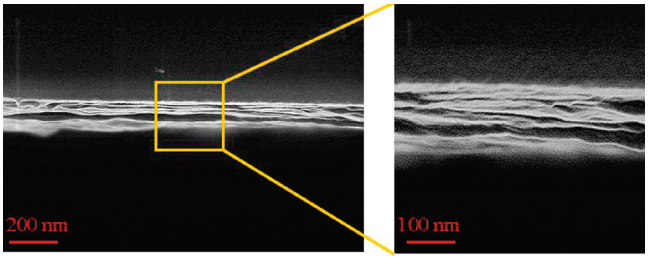

Figure 5. FESEM images of cross section of a 50-bilayer PVA/GO composites with different magnification.

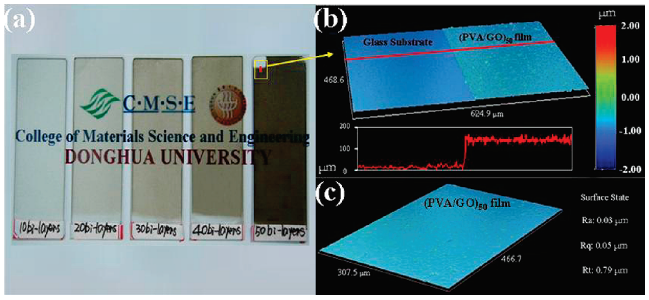

Figure 6. (a) Optical images of $(PVA/GO)_n$ composites deposited on cleaned glass substrates with gradually increasing deposited cycles, n = 10, 20, 30, 40, and 50, and the surface topography of $(PVA/GO)_{50}$ ultrathin film with the thickness (b) and the roughness (c).

The XRD patterns in Figure 8 of the multilayer $(PVA/GO)_n$ ultrathin films illustrate the evolution of a Bragg peak at 2θ = 4.9°, indicating the average repeating distance of ~1.5 nm. Therefore, the average thickness of one (PVA/GO) unit is about 3 nm. Although it is broad, the peak intensity and symmetry progressively increase with the increase of the bilayer number, further verifying the successful multilayer buildup. This diffraction feature is attributed to a so-called superlattice reflection of the periodic nanostructure of inorganic nanosheets and organic polymer, and its enhancement with increasing numbers of deposition cycles indicates the progressive growth of its repeating assemblies.[31,45,46] The periodicity of ~3 nm is consistent with the observation in FESEM cross-section image of the $(PVA/GO)_{50}$ film in Figure 5.

3.3. Mechanical Properties of Multilayer $(PVA/GO)_n$ Films. The typical force−displacement profiles with loading−hold−unloading courses of pure PVA films and LBL assembling $(PVA/GO)_{300}$ film are shown in Figure 9, which is measured by the TriboIndenter in-situ nanomechanical test system. Upon loading, the force is incremented at constant velocities and the maximum value is 150 μm. The penetration depth represents the contributions from the elastic and plastic displacements. It is noted that the penetration depth of $(PVA/GO)_{300}$ film is decreased remarkably, indicating an enhancement of nanocomposite's resistance to indentation. That is, the softer material surface requires lower normal loads to induce a comparable indenter penetration. Upon holding time with 5 s, at which the peak loads are kept constant, a creep is clearly observed in the maximum hold segments for pure PVA film. During the unloading, the force is removed and the elastic displacement is recovered. It is shown that the ending displacement of pure PVA film is much larger than that of $(PVA/GO)_{300}$ film. Furthermore, the initial unloading stiffness of the $(PVA/GO)_{300}$ film, as represented by the slope of the unloading curve, is larger than

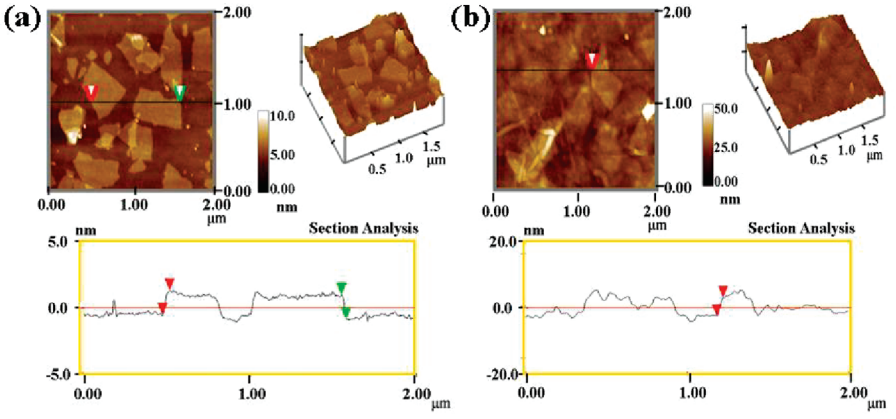

Figure 7. AFM tapping-mode images of (a) 1-bilayer PVA/GO ultrathin film deposited onto silicon wafer substrate with superimposed cross-section measurements taken along the red line, indicating a sheet thickness of ~1.5 nm. (b) 5-bilayer PVA/GO ultrathin film deposited onto silicon wafer substrate with superimposed cross-section measurements taken along the red line, indicating a sheet thickness of ~7.0 nm.

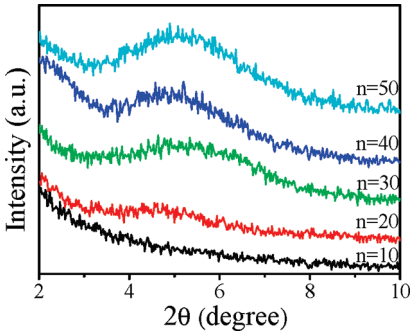

Figure 8. XRD curves of the ultrathin films of $(PVA/GO)_n$ assembled on quartz glass slides with increasing deposited cycles.

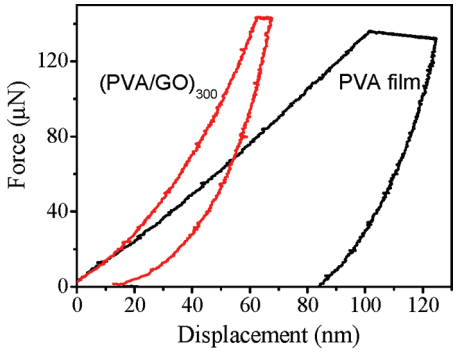

Figure 9. Typical loading−hold−unloading curves of pure PVA film and LBL assembling $(PVA/GO)_{300}$ film.

Table 1. Average Values of Elastic Modulus and Hardness for PVA and Nanocomposites

samples	E_r (GPa)	hardness (GPa)
pure PVA film	8.88 ± 0.02	0.34 ± 0.01
$(PVA/GO)_{300}$	17.64 ± 0.02	1.15 ± 0.03

that of pure PVA film, suggesting the increase of elastic modulus. The average values of elastic modulus (E_r) and hardness derived by the Oliver and Pharr's method[47] listed in Table 1 exhibit a significant enhancement of mechanical properties of LBL assembling PVA/GO nanocomposites; that is, a 98.7% improvement of E_r and a 240.4% increase of hardness. A similar tendency for E_r and hardness in the case of graphene-based PVA composites were also reported by Das et al.,[48] a maximum increase of 35% and 45% in the E_r and hardness of PVA with 0.6 wt % graphene loading, respectively. The reasons for our remarkable increase in the mechanical properties are attributed to the nanometer-level dispersion and the orientation of GO nanosheets in the polymer matrices. The degree of structural organization by the LBL process of the nanoplatelets in the composite can maximize the number of graphene oxide/PVA interaction and constrain the polymer chain motion, which results in a highly efficient particle-to-matrix-to-particle load transfer between the polymer phase and the stiff graphene platelets.

4. Conclusions

In summary, the uniform ultrathin multilayer $(PVA/GO)_n$ films with high homogeneity and orientation were successfully fabricated by the LBL assembly technique driven by hydrogen-bonding interaction. The thickness of per bilayer is about 3 nm. The fully exfoliated and well-dispersed GO nanosheets have a high degree of planar orientation in the lamella structure films, resulting in a significant enhancement of the mechanical properties for the LBL nanocomposites: Compared with a parallel pure PVA sample, the values are a 98.7% improvement of E_r and a 240.4% increase of hardness. The remarkable increases in the mechanical properties are attributed to the nanometer-level assemblies and the orientation of GO nanosheets in the polymer matrices. This work opens up a broad avenue for the molecular engineering of nanocomposites and the high degree of control over their nanoscale orientation.

Acknowledgment. Financial support of this work is provided by NSFC (50873021, 50925312), Shuguang (09SG30), Program for New Century Excellent Talents in University (NCET-06-0421), Shanghai Leading Academic Discipline Project (B603), and the 111 Project (111-2-04).

References and Notes

(1) Lee, C.; Wei, X. D.; Kysar, J. W.; Hone, J. *Science* **2008**, *321*, 385.
(2) Gómez-Navarro, C.; Burghard, M.; Kern, K. *Nano Lett.* **2008**, *8*, 2045.
(3) Balandin, A. A.; Ghosh, S.; Bao, W. Z.; Calizo, I.; Teweldebrhan, D.; Miao, F.; Lau, C. N. *Nano Lett.* **2008**, *8*, 902.
(4) Bolotin, K. I.; Sikes, K. J.; Jiang, Z.; Klima, M.; Fudenberg, G.; Hone, J.; Kim, P. *Solid State Commun.* **2008**, *146*, 351.
(5) Stoller, M. D.; Park, S. J.; Zhu, Y. W.; An, J. H.; Ruoff, R. S. *Nano Lett.* **2008**, *8*, 3498.
(6) Zhang, Y. B.; Tan, Y. W.; Stormer, H. L.; Kim, P. *Nature* **2005**, *438*, 201.
(7) Shen, J.; Hu, Y.; Shi, M.; Lu, X.; Qin, C.; Li, C.; Ye, M. *Chem. Mater.* **2009**, *21*, 3514.
(8) Shen, J. F.; Hu, Y.; Li, C.; Qin, C.; Shi, M.; Ye, M. *Langmuir* **2009**, *25*, 6122.
(9) Mkhoyan, K. A.; Contryman, A. W.; Silcox, J.; Stewart, D. A.; Eda, G.; Mattevi, C.; Miller, S.; Chhowalla, M. *Nano Lett.* **2009**, *9*, 1058.
(10) Stankovich, S.; Dikin, D. A.; Dommett, G. H. B.; Kohlhaas, K. M.; Zimney, E. J.; Stach, E. A.; Piner, R. D.; Nguyen, S. T.; Ruoff, R. S. *Nature* **2006**, *442*, 282.
(11) Watcharotone, S.; Dikin, D. A.; Stankovich, S.; Piner, R.; Jung, I.; Dommett, G. H. B.; Evmenenko, G.; Wu, S.; Chen, S. F.; Liu, C. P.; Nguyen, S. T.; Ruoff, R. S. *Nano Lett.* **2007**, *7*, 1888.
(12) Park, S.; Lee, K. S.; Bozoklu, G.; Cai, W.; Nguyen, S. T.; Ruoff, R. S. *ACS Nano* **2008**, *2*, 572.
(13) Wang, S.; Tambraparni, M.; Qiu, J.; Tipton, J.; Dean, D. *Macromolecules* **2009**, *42*, 5251.
(14) Li, D.; Muller, M. B.; Gilje, S.; Kaner, R. B.; Wallace, G. G. *Nature Nanotechnol.* **2008**, *3*, 101.
(15) Stankovich, S.; Piner, R. D.; Nguyen, S. T.; Ruoff, R. S. *Carbon* **2006**, *44*, 3342.
(16) Stankovich, S.; Piner, R. D.; Chen, X.; Wu, N.; Nguyen, S. T.; Ruoff, R. S. *J. Mater. Chem.* **2006**, *16*, 155.
(17) Liang, J.; Huang, Y.; Zhang, L.; Wang, Y.; Ma, Y.; Guo, T.; Chen, Y. *Adv. Funct. Mater.* **2009**, *19*, 2297.
(18) Han, J. B.; Lu, J.; Wei, M.; Wang, Z. L.; Duan, X. *Chem. Commun.* **2008**, *41*, 5188.
(19) Jiang, C.; Tsukruk, V. V. *Adv. Mater.* **2006**, *18*, 829.
(20) Decher, G.; Hong, J. D. *Makromol. Chem., Macromol. Symp.* **1991**, *46*, 321.
(21) Wang, L.; Wang, Z.; Zhang, X.; Shen, J. *Macromol. Rapid Commun.* **1997**, *18*, 509.
(22) Stockton, W. B.; Rubner, M. F. *Macromolecules* **1997**, *30*, 2717.
(23) Wang, L.; Fu, Y.; Wang, Z.; Fan, Y.; Zhang, X. *Langmuir* **1999**, *15*, 1360.
(24) Hao, E.; Lian, T. *Langmuir* **2000**, *16*, 7879.
(25) Such, G. K.; Quinn, J. F.; Quinn, A.; Tjipto, E.; Caruso, F. *J. Am. Chem. Soc.* **2006**, *128*, 9318.
(26) Buck, M. E.; Zhang, J.; Lynn, D. M. *Adv. Mater.* **2007**, *19*, 3951.
(27) Zhou, M.; Liu, X.; Zhang, B.; Zhu, H. *Langmuir* **2008**, *24*, 11942.
(28) Seo, J.; Lutkenhaus, J. K.; Kim, J.; Hammond, P. T.; Char, K. *Langmuir* **2008**, *24*, 7995.
(29) Chen, D.; Wang, X.; Liu, T.; Wang, X.; Li, J. *ACS Appl. Mater. Interfaces* **2010**, *2*, 2005.
(30) Podsiadlo, P.; Kaushik, A. K.; Shim, B. S.; Agarwal, A.; Tang, Z.; Waas, A. M.; Arruda, E. M.; Kotov, N. A. *J. Phys. Chem. B* **2008**, *112*, 14359.

(31) Zhuk, A.; Pavlukhina, S.; Sukhishvili, S. A. *Langmuir* **2009**, *25*, 14025.
(32) Kharlampieva, E.; Kozlovskaya, V.; Sukhishvili, S. A. *Adv. Mater.* **2009**, *21*, 3053.
(33) Podsiadlo, P.; Kaushik, A. K.; Arruda, E. M.; Waas, A. M.; Shim, B. S.; Xu, J.; Nandivada, H.; Pumplin, B. G.; Lahann, J.; Ramamoorthy, A.; Kotov, N. A. *Science* **2007**, *318*, 80.
(34) Zhao, X.; Zhang, Q.; Chen, D.; Lu, P. *Mcromolecules* **2010**, *43*, 2357.
(35) Hummers, W. S.; Offeman, R. E. *J. Am. Chem. Soc.* **1958**, *80*, 1339.
(36) Paredes, J. I.; Villar-Rodil, S.; Martinez-Alonso, A.; Tascon, J. M. D. *Langmuir* **2008**, *24*, 10560.
(37) Lerf, A.; Buchsteiner, A.; Pieper, J.; Schottl, S.; Dekany, I.; Szabo, T.; Boehm, H. P. *J. Phys. Chem. Solids* **2006**, *67*, 1106.
(38) Chieu, T. C.; Dresselhaus, M. S. *Phys. Rev. B* **1982**, *26*, 5867.
(39) Wang, S.; Zhang, Y.; Abidi, N.; Cabrales, L. *Langmuir* **2009**, *25*, 11078.
(40) Cai, D.; Song, M. *J. Mater. Chem.* **2007**, *17*, 3678.
(41) Stankovich, S.; Dikin, D. A.; Piner, R. D.; Kohlhaas, K. A.; Kleinhammes, A.; Jia, Y.; Wu, Y.; Nguyen, S. T.; Ruoff, R. S. *Carbon* **2007**, *45*, 1558.
(42) Waltman, R. J.; Pacansky, J.; Bates, C. W. *Chem. Mater.* **1993**, *5*, 1799.
(43) Decher, G. *Science* **1997**, *277*, 1232.
(44) Tang, Z.; Kotov, N. A.; Magonov, S.; Ozturk, B. *Nature Mater.* **2003**, *2*, 413.
(45) Li, L.; Ma, R.; Ebina, Y.; Iyi, N.; Sasaki, T. *Chem. Mater.* **2005**, *17*, 4386.
(46) Liu, Z.; Ma, R.; Osada, M.; Iyi, N.; Ebina, Y.; Takada, K.; Sasaki, T. *J. Am. Chem. Soc.* **2006**, *128*, 4872.
(47) Oliver, W. C.; Pharr, G. M. *J. Mater. Res.* **1992**, *7*, 1564.
(48) Das, B.; Prasad, K. E.; Ramamurty, U.; Rao, C. N. R. *Nanotechnology* **2009**, *20*, 125705.